Inorganic Chemistry

pubs.acs.org/IC Article

Trifluoromethylated Phenanthroline Ligands Reduce Excited-State Distortion in Homoleptic Copper(I) Complexes

Maksim Y. Livshits, Brian J. Reeves, Nicholas J. DeWeerd, Steven H. Strauss, Olga V. Boltalina,* and Jeffrey J. Rack*



Cite This: Inorg. Chem. 2020, 59, 2781-2790



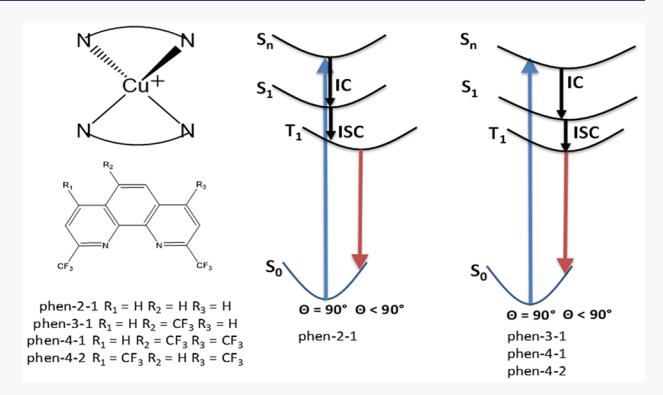
ACCESS I

III Metrics & More

Article Recommendations

Supporting Information

ABSTRACT: We report the synthesis and excited-state dynamics for a series of homoleptic copper(I) trifluoromethylated phenanthroline complexes with two, three, and four trifluoromethyl functional groups. Our analysis of the steady-state absorbance and emission, transient-absorption spectroscopy, and electronic-structure-theory calculations results enable in-depth analysis of the pseudo-Jahn—Teller distortion inhibition from increased steric hindrance of the trifluoromethyl functional group relative to the prototypical dimethyl phenanthroline complex. Surprisingly, our results demonstrate that the greatest degree of pseudo-Jahn—Teller distortion inhibition is achieved with trifluoromethylation of only the 2 and 9 positions by an unusual combination of steric hindrance and stabilization of a nondistorted ¹MLCT manifold observed by transient kinetic



lifetimes and optimized excited-state structures. The intersystem-crossing (ISC) lifetime for the 2,9-bis(trifluoromethyl)-1,10-phenanthroline Cu(I) complex is 69 ps, while the triplet excited-state lifetime and emission quantum yield are 106 ns and 4×10^{-3} , respectively. Further trifluoromethylation of the phenanthroline yields a greater σ bond inductive withdrawing force on the phenanthroline nitrogens, ultimately resulting in weaker coordination to the copper. Last, the surprising success of the 2,9-bis(trifluoromethyl)-1,10-phenanthroline Cu(I) complex by adjusting both ligand sterics and electronic properties outlines a new strategy for developing long-lived Cu(I) charge-transfer complexes.

■ INTRODUCTION

Polypyridyl Cu(I) complexes featuring low lying metal-toligand charge transfer excited-states have drawn much attention due to their similarity to well-studied Ru(II) counterparts. 1-7 Recent reports highlight the use of Cu(I) complexes in photoredox,8 OLEDs,2 and dye-sensitized solar cells.^{1,3} Moreover, unlike many photoactive first-row transition metals (Cr, Fe, 10,11 and Co 12), these Cu(I) complexes do not suffer from lower-lying metal centered or d-d states, which act to quench the charge-transfer excited state on a subpicosecond to picosecond time scale. However, initial experiments by McMillin and co-workers demonstrated that the roomtemperature emission lifetime and quantum yield (QY) for Cu(I) polypyridine MLCT excited states are smaller than those for related ruthenium complexes, as well as extremely sensitive to the solvent Lewis basicity. ^{6,13,14} These results have led to the conclusion that the Cu(I) MLCT excited state, consisting of a formally oxidized Cu(II) and reduced ligand π orbital, undergoes a pseudo-Jahn-Teller distortion resulting in an exposed metal center enabling solvent coordination to shorten the excited-state lifetime. More recent experiments and calculations have demonstrated that the pseudo-Jahn-Teller distortion originating from the Cu(I) d^{10} to Cu(II) d^{9}

oxidation occurs on a subpicosecond time scale lowering the interligand dihedral angle, which in turn relaxes the symmetry of the complexes from pseudo T_d to D_2 , creating more nonradiative excited-state deactivation channels. ^{15–19}

A number of attempts have been made to lessen the degree of the pseudo-Jahn—Teller distortion in the excited state by adding steric hindrance to the phenanthroline ligand. One strategy was to derivatize the phenanthroline (phen) in the 2,9 or 3,8 positions with bulkier functional groups. This strategy has been pursued by a number of researchers and has yielded much success in extending the MLCT lifetime from nanoseconds to microseconds.^{20–26} In aggregate, all reports demonstrated that inhibition of the pseudo-Jahn—Teller distortion yields a shift to higher energy of the emission maxima, an increase in the emission QY, and an elongation of the excited-state lifetime measured by time-resolved emission and transient absorption spectroscopy. It should be noted that

Received: October 27, 2019 Published: February 12, 2020



Scheme 1. Bond Line Structure(s) of [Cu(NN)₂]⁺ (Left) Complexes Utilized in This Study^a

^aHere, NN is 2,9-dimethyl-1,10-phenanthroline, phen-2-1, phen-3-1, phen-4-1, and phen-4-2.

the largest changes in the inhibition of the pseudo-Jahn—Teller distortion came from increasing the steric bulk of the 2,9 positions from methyl to 2,9-diyl(bis(methanylylidene))bis(2-methylaniline) or 2,9-di(sec-butyl)-3,4,7,8-tetramethyl.^{22,25}

An alternative strategy for the inhibition of the pseudo-Jahn-Teller distortion is by substitution of the 2,9 methyl groups with 2,9 trifluoromethyls (CF₃).²⁷ While inhibition of the pseudo-Jahn-Teller distortion was not the original goal for the trifluoromethylation of phen, it was noticed that the interligand dihedral angle (θ) in the ground state is 87° (close to idealized 90°) compared to the 72–83° of the 2,9-dimethyl-1,10-phenanthroline (dmp). Further crystal structure comparison of the Cu(I) 2,9-trifluoromethyl-1,10-phenanthroline (bfp or phen-2-1) complex with different anions calculated a ground state θ spread from 86 to 90°. The anion dependence of the [Cu^I(NN)₂]⁺ single crystal structure has been observed for many Cu(I) complexes and is ascribed to crystal stress. To complement the ground state change in θ , the $[Cu^{I}(phen-2-1)_{2}]^{+}$ complex also exhibits a blue shift in the emission maxima, enhanced QY (almost 10 times), and elongated emission lifetime relative to $[Cu^{I}(dmp)_{2}]^{+}$, similar to the other $[Cu^{I}(NN)_{2}]^{+}$ complexes with sterically bulkier phen.

These results of the [Cu^I(phen-2-1)₂]⁺ are expected as CF₃ groups are bulkier than CH₃ groups. It would be expected that CF₃ groups would also lower the ligand LUMO energy, resulting in a slightly lower energy MLCT maximum as observed in trifluoromethylated polypyridyl ruthenium(II) complexes.³¹ Unfortunately, little excited state investigation has been performed on the [Cu^I(phen-2-1)₂]⁺ beyond ground-state electronic absorption, emission spectra, and emission lifetimes. In addition, [Cu^I(NN)₂]⁺ complexes with more than two CF₃ groups have not been synthesized or studied prior to this work. While CF₃ substitutions at the 2,9-position of phen represent an interesting opportunity to increase steric bulk, the use of this steric bulk with more electron withdrawing ligands has not been studied.

Herein, we report the synthesis and excited-state dynamics for a series of trifluoromethylated copper(I) phenanthroline complexes with two, three, and four CF_3 groups, in which all phen ligands are substituted at the 2 and 9 positions with CF_3 groups (Scheme 1). We report the excited-state evolution for all complexes, examining the effect of the number and position of CF_3 groups on the phen core on the excited state pseudo-Jahn–Teller distortion using ultrafast pump–probe and nanosecond flash photolysis transient absorption. We also performed preliminary restricted and unrestricted DFT and TDDFT electronic structure calculations to optimize the ground state (S_0) , lowest energy triplet (T_1) , and singlet (S_1)

excited states as well as the singlet state with the largest transition oscillator strength from the ground state (S_n) . In addition, since all of the trifluoromethylated ligands have identical steric bulk at the 2 and 9 positions, it is possible to make correlations between the number of electron withdrawing groups and excited-state lifetimes and quantum yields.

EXPERIMENTAL SECTION

Synthesis of 2,9-Bis(trichloromethyl)-1,10-phenanthroline. On the basis of literature prep, 32 neocuproine hemihydrate (500 mg, 2.30 mmol, 1 equiv) and N-chlorosuccinimide (4.61 g, 34.52 mmol, 15 equiv) were added to a 300 mL round-bottom flask. Chloroform (150 mL) was added to the flask, and the reaction mixture was refluxed for 6 h followed by cooling to room temperature. The solvent was removed *in vacuo*, resulting in a yellow solid. Saturated sodium carbonate (100 mL) and chloroform (40 mL) were then added. The product was extracted into chloroform (2 × 20 mL). The organic layer was then washed with DI water, 6 × 50 mL. The solvent was again removed *in vacuo*, resulting in a yellow solid. The product was then purified on silica (eluent 2:1 chloroform/hexanes).

Synthesis of phen-2–1. On the basis of a modified literature prep, 32 2,9-bis(trichloromethyl)-1,10-phenanthroline (150 mg, 0.36 mmol) was combined with antimony(III) fluoride (1.5 g, 8.4 mmol) and ground with a mortar and pestle. The mixture was then added to a 50 mL round-bottom flask and fitted with a reflux condenser under $N_{2(g)}$. Heat was applied until a melt formed. The mixture was heated for one more minute and allowed to cool to room temperature. Sodium hydroxide (5M) was added to the flask and transferred to a separatory funnel. Dichloromethane, 50 mL, was added and transferred to a separatory funnel. The product was extracted with dichloromethane (3 × 20 mL), dried on sodium sulfate, and passed through silica gel. The solvent was removed *in vacuo*, resulting in a white crystalline solid (39% yield). ^{19}F NMR: δ –69.9 (singlet, 6F). ^{1}H NMR: δ 8.5 (doublet, J = 8 Hz, 2H); 8.0 (doublet, J = 8 Hz, 2H); 8.0 (singlet, 2H).

Synthesis and Purification of phen-4–1, phen-4–2, and phen-3–1. The compound phenanthroline monohydrate (251.5 mg, 1.27 mmol) was added to a glass ampule. CF_3I gas (10 equiv) was introduced and cooled to -78 °C, and the ampule was sealed under a vacuum (10^{-4} Torr). The ampule was heated to 330 °C for 10 h and subsequently cooled to room temperature. The ampule was opened, and soluble trifluoromethylated phenanthroline derivatives were extracted with dichloromethane. The dichloromethane solution was washed with a 10% solution of sodium thiosulfate to remove iodine.

Primary separation of the phenanthroline $(CF_3)_n$ derivatives was performed on a semipreparative Cosmosil Buckyprep HPLC column with acetonitrile as the eluent (Figure S1). This separation afforded five major fractions containing phen $(CF_3)_n$ derivatives. Of the five fractions, two fractions were able to be separated into pure isomers of tris- and tetra-substituted phenanthroline derivatives. Secondary separation of fraction 2 (4.0–4.8 min) in MeOH at 5 mL/min led to the isolation of phen-3–1 (0.7 mg, 0.002 mmol, 0.16% yield) at 16.5–17.5 min (Figure S2). Fraction 3 was sonicated in heptane, and

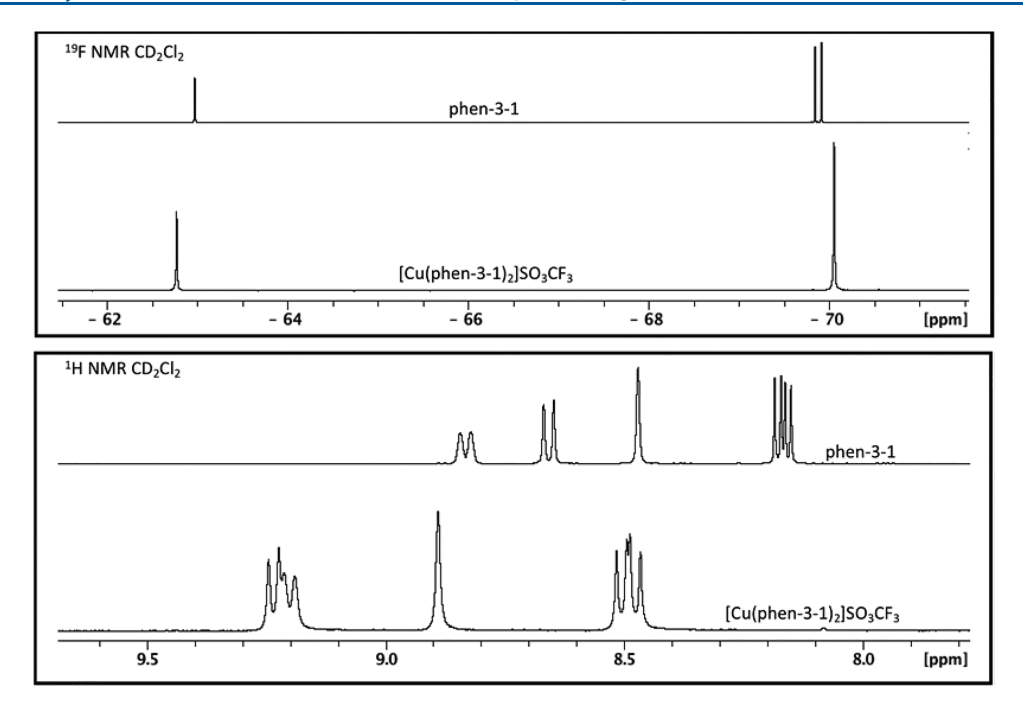


Figure 1. (Top) ¹⁹F NMR spectra of phen-3-1 and [Cu(phen-3-1)₂]SO₃CF₃. (Bottom) ¹H NMR spectra of phen-3-1 and [Cu(phen-3-1)₂]SO₃CF₃.

insoluble materials were filtered off (approximately 2 mg, which did not show observable NMR signals when dissolved in $CDCl_3$). The heptane soluble material (F3H) was then separated in a 25:75 toluene/heptane mixture. This significantly improved the separation and yielded two major compounds, phen-4–2 (2.7 mg, 0.0060 mmol, 0.5% yield) and phen-4–1 (14.1 mg, 0.0311 mmol, 2.4% yield), represented in the chromatogram as A (6.5–7.5 min) and B (7.5–8.2 min), respectively (Figure S3). The highest yielding isolable compound from the mixture was phen-4–1.

phen-3–1. ¹⁹F NMR: δ –63.5 (singlet, 3F); –70.3 (singlet, 3F); –70.3 (singlet, 3F). ¹H NMR: δ 8.8 (doublet, J = 9 Hz 1H); 8.6 (doublet, J = 9 Hz 1H); 8.4 (singlet, 1H), 8.1 (multiplet, 2H).

phen-4–1. ¹⁹F NMR: δ –63.4 (singlet, 3F); –63.7 (singlet, 3F) –70.4 (singlet, 3F); –70.5 (singlet, 3F). ¹H NMR: δ 8.9 (doublet, J = 9 Hz 1H); 8.7 (singlet, 1H); 8.4 (singlet, 1H); 8.2 (doublet, J = 9 Hz 1H).

phen-4–2. ¹⁹F NMR: δ –63.8 (singlet, 6F); –70.3 (singlet, 6F). ¹H NMR: δ 8.5 (singlet, 2H); 8.4 (singlet, 2H).

Synthesis of [Cu(phen-4–1)₂]SO₃CF₃. A 0.041 M solution of PHEN-4–1 in dichloromethane-d₂ (0.5 mL, 0.021 mmol) was added to an air-free NMR tube with 0.9 mL of dichloromethane-d₂. The ¹⁹F NMR and the ¹H NMR spectra of the ligand were recorded. Copper(I) trifluoromethanesulfonate toluene complex (55 mg, 0.106 mmol) was added to the NMR tube, and the NMR spectra were recorded again. The mixture was filtered and dried *in vacuo*, yielding a dark orange solid (7.5 mg, 0.0067 mmol, 65% yield). ¹⁹F NMR: δ –62.5 (singlet, 3F); –62.9 (singlet, 3F); –69.9 (singlet, 3F); –70.0 (singlet, 3F). ¹H NMR: δ 9.3 (doublet, J = 8 Hz 1H); 9.0 (singlet, 1H); 8.8 (singlet, 1H); 8.6 (doublet, J = 9 Hz 1H). ESI+ MS (m/z): 967.08 (calcd mass: 966.97).

Synthesis of [Cu(phen-3–1)₂]SO₃CF₃. A 0.0275 M solution of phen-3–1 in dichloromethane-d₂ (0.5 mL, 0.0138 mmol) was added to an air-free NMR tube. Copper(I) trifluoromethanesulfonate toluene complex (40 mg, 0.077 mmol) was added and placed on a rotating motor to provide mixing. The mixture was filtered and dried *in vacuo*, yielding a dark orange solid (4.8 mg, 0.0049 mmol, 71% yield). ¹⁹F NMR: δ –62.8 (singlet, 3F); –70.1 (singlet, 6F). ¹H NMR: δ 9.2 (doublet, J = 9 1H); 9.2 (doublet, J = 9 1H); 8.9 (singlet, 1H), 8.5 (multiplet, 2H). ESI+ MS (m/z): 831.17 (calcd mass: 830.99).

Synthesis of [Cu(phen-4–2)₂]SO₃CF₃. A 0.037 M solution of phen-4–2 in dichloromethane-d₂ (0.1 mL, 3.7 μ mol) was added to an air-free NMR tube with 0.9 mL of dichloromethane-d₂. Copper(I) trifluoromethanesulfonate toluene complex (10 mg, 0.019 mmol) was added to the NMR tube, and the NMR spectra were recorded again. The mixture was filtered and dried *in vacuo* yielding a dark orange solid (0.3 mg, 0.27 μ mol, 15% yield). ¹⁹F NMR: δ –62.9 (singlet, 6F), –69.7 (singlet, 6F). ¹H NMR: δ 8.8 (singlet, 2H); 8.8 (singlet, 2H). ESI+ MS (m/z): 966.90 (calcd mass: 966.97).

Synthesis of [Cu(phen-2–1)₂**ISO**₃**CF**₃. A 0.14 M solution of phen-2–1 in dichloromethane-d₂ (0.1 mL, 0.014) was added to an air-free NMR tube with 0.5 mL of dichloromethane-d₂. The copper(I) trifluoromethanesulfonate toluene complex (16 mg, 0.031 mmol) was added and placed on a rotating motor to provide mixing. The mixture was filtered and dried *in vacuo* yielding a dark orange solid (3.5 mg, 0.0041 mmol, 59% yield). ¹⁹F NMR: δ –69.9 (singlet, 6F). ¹H NMR: δ 9.0 (doublet, J = 8 Hz, 2H); 8.4 (singlet, 2H); 8.4 (doublet, J = 8 Hz, 2H). ESI+ MS (m/z): 695.25 (calc. mass: 695.02).

Instrumentation details and DFT methods (including benchmark discussion) are found in the Supporting Information.

RESULTS

Ligand and Complex Structures. The ligands shown in Scheme 1 were synthesized in a single step reaction and were isolated via HPLC, solubility differences, and crystallization techniques. NMR spectra were collected for the ligands and for the copper complexes, and mass spectra were collected for the copper complexes (Figure 1 and S4–S28). There is a very slight shift in the ¹⁹F NMR spectra from the phen-3–1 ligand in comparison to the complex (Figure 1). A similar result is observed for phen-4–1 and phen-4–2, and that of phen-2–1 is shown in the SI. In the case of phen-3–1, the CF₃ groups substituted at the 2 and 9 positions (approximately –70 ppm) become accidentally isochronous when the ligand is bound in the Cu(I) complex. A much more noticeable shift is observed in the ¹H NMR spectra comparing ligand and complex (Figure 1).

Single-crystal X-ray structures were obtained for [Cu(phen-3-1)₂]SO₃CF₃ and [Cu(phen-4-1)₂]SO₃CF₃ as shown in

Figure 2. High quality single crystals of [Cu(phen-4–2)₂]SO₃CF₃ were not obtained. The dihedral ligand angle

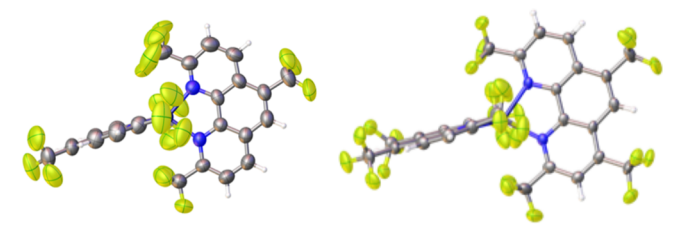


Figure 2. Single crystal XRD structures for $[Cu(phen-3-1)_2]^+$ (left) and $[Cu(phen-4-1)_2]^+$ (right). Triflate anions not shown for clarity. Thermal ellipsoids are plotted at a default 50% probability.

for $[Cu(phen-3-1)_2]^+$ is 86.1°. The dihedral ligand angle for $[Cu(phen-4-1)_2]^+$ is 85.4°. The Cu-N bond lengths for $[Cu(phen-4-1)_2]^+$ are 2.054, 2.048, 2.052, and 2.051 Å. The Cu-N bond lengths for $[Cu(phen-3-1)_2]^+$ are 2.037, 2.047, 2.038, 2.033 Å.

Electronic Absorption and Emission Spectroscopy. The absorption spectra of the trifluoromethyl phen [Cu- $(NN)_2$]⁺ complexes (Scheme 1) investigated here display MLCT absorption maxima at 463, 464, 481, and 482 nm for [Cu(phen-2-1)₂]⁺, [Cu(phen-3-1)₂]⁺, [Cu(phen-4-1)₂]⁺, and [Cu(phen-4-2)₂]⁺, respectively (Figure 3A-C). A higher

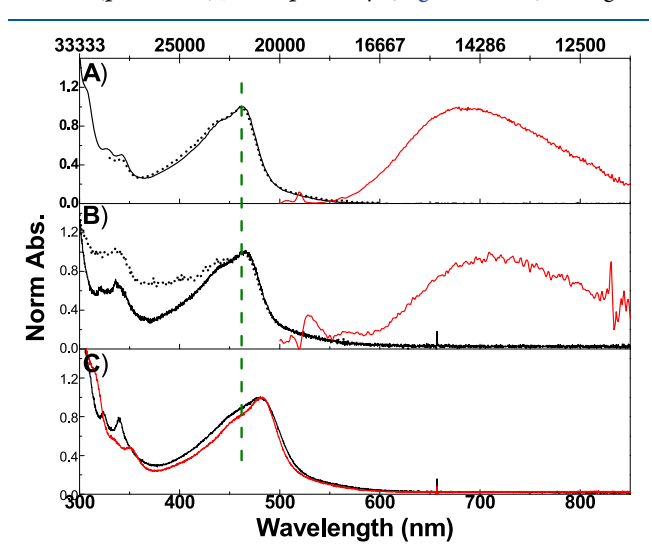


Figure 3. (A) Normalized electronic absorption (black solid line), emission (red), and excitation (black scatter line) spectra for $[Cu(phen-2-1)_2]OTf$ in 1,2-dichloroethane. (B) Normalized electronic absorption (solid black), emission (red), and excitation (scatter black) spectra for $[Cu(phen-3-1)_2]OTf$ in 1,2-dichloroethane. (C) Normalized electronic absorption of $[Cu(phen-4-1)_2]OTf$ (black) and $[Cu(phen-4-2)_2]OTf$ (red) in 1,2-dichloroethane. The dashed green line is added to highlight differences in the absorption spectra.

energy MLCT transition is also observed at 341, 338, 339, and 351 nm for $[Cu(phen-2-1)_2]^+$, $[Cu(phen-3-1)_2]^+$, $[Cu(phen-4-1)_2]^+$, and $[Cu(phen-4-2)_2]^+$, respectively (Figure 3A–C). Last, a low energy tail is observed in each complex from 500 to 600 nm. The emission spectra for $[Cu(phen-2-1)_2]^+$ and $[Cu(phen-3-1)_2]^+$ depict a broad featureless transition with maxima near 685 and 718 nm, respectively, assignable to a ligand-to-metal charge transfer (LMCT) transition. The excitation profiles (dotted traces, Figure 3A,B) for $[Cu-1)_2$

(phen-2–1)₂]⁺ and [Cu(phen-3–1)₂]⁺ complexes overlap well with their corresponding absorption spectra, replicating all spectral features. The [Cu(phen-4–1)₂]²⁺ and [Cu(phen-4–2)₂]²⁺ show evidence of decomposition upon long-term exposure to light and thus their emission spectra were not collected (Figure S43).

Pump Probe Transient Absorption Spectroscopy. The pump—probe transient spectra of $[Cu(phen-2-1)_2]^+$ and $[Cu(phen-3-1)_2]^+$ are shown in Figure 4A and B, respectively.

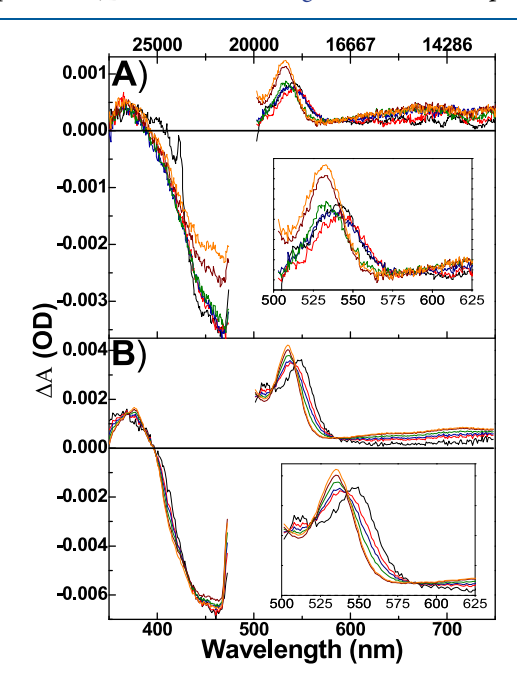


Figure 4. Ultrafast pump probe transient absorption spectra for $[Cu(phen-2-1)_2]OTf$ (A) and $[Cu(phen-3-1)_2]OTf$ (B) collected in 1,2-dichloroethane. Insets: Enhanced 500 to 625 nm region for $[Cu(phen-2-1)_2]OTf$ and $[Cu(phen-3-1)_2]OTf$ to highlight spectral changes. The spectra are taken at 0.3 ps (black), 0.75 ps (red), 2.5 ps (blue), 10 ps (green), 50 ps (brown), and 100 ps (orange).

The gross features of the $[Cu(NN)_2]^+$ complexes consist of two photoinduced excited-state absorption (ESA) transitions from ~350 to 400 nm and from ~500 to 750 nm, as well as a negative peak ranging from 400 to 500 nm. The maxima of the two ESAs appear at 365 and 371 nm as well as 532 and 535 nm for $Cu(phen-2-1)_2$ and $[Cu(phen-3-1)_2]^+$, respectively. The maxima of the negative signal of $[Cu(phen-2-1)_2]^+$ and $[Cu(phen-3-1)_2]^+$ are observed at 469 and 463 nm, respectively. Time-resolved resonance Raman measurements have previously been assigned to the excited state "doublepeak" absorption from 500 to 625 nm to reduced phenanthroline (phen⁻) $\pi^* \to \pi^*$ ligand localized transition in $[Cu(NN)_2]^+$ complexes.³³ For this reason, the ESA region from ~500 to 625 is enhanced to highlight important spectral changes in the temporal response at these wavelengths (Figure 4, insets). The negative signal is assigned to the depletion or bleach of the ground state (GSB). The long, low amplitude featureless absorption from 625 to 750 nm has been assigned to LMCT transition. Nanosecond flash photolysis transient absorption spectra for the [Cu(phen-2-1)₂]⁺ and [Cu(phen- $(3-1)_2$ complexes are consistent with the final spectra from the pump-probe transient absorption experiment, inferring that no intermediate excited state exists between the two

Table 1. Absorbance, Excited-State Absorbance, and Emission Global Fitting Lifetimes As Well As Emission Quantum Yield

	$[Cu(dmp)_2]^+$	$[Cu(phen-2-1)_2]^+$	$[Cu(phen-3-1)_2]^+$	$[Cu(phen-4-1)_2]^+$	$[Cu(phen-4-2)_2]^+$
λ_{\max} (nm)	457	463	464	481	482
τ_1 (ps)	0.3 (fixed) ^a				4 ^a
$\tau_2(\mathrm{ps})$	54 ± 15	69 ± 5	6.0 ± 2.3	10.0 ± 7.0	150 ± 20
$\tau_3(\mathrm{ns})$	66.6 ± 2.1	106 ± 2	68.3 ± 0.6	15.5 ± 1.7^{b}	
$ au_{ m em}(m ns)$	52.0 ± 1.4	98 ± 2	82 ± 2^b	17.9 ± 2.2^{b}	
$\Phi_{\mathtt{p}}$	3.5×10^{-4}	4.0×10^{-3}	1.1×10^{-3}		

"Note, τ_1 is fixed from single wavelength kinetic time constant to yield a more accurate fit of τ_2 . "Time constant found in single wavelength kinetics.

experiments (Figures S33 and S36). The time constants from the multiexponential fitting of the pump—probe transient absorption and nanosecond flash photolysis experiments are summarized in Table 1 with the data found in the Supporting Information (Figures S32 to S37).

The pump-probe transient spectra of $[Cu(phen-4-1)_2]^+$ and $[Cu(phen-4-2)_2]^+$ are shown in Figure 5A and B,

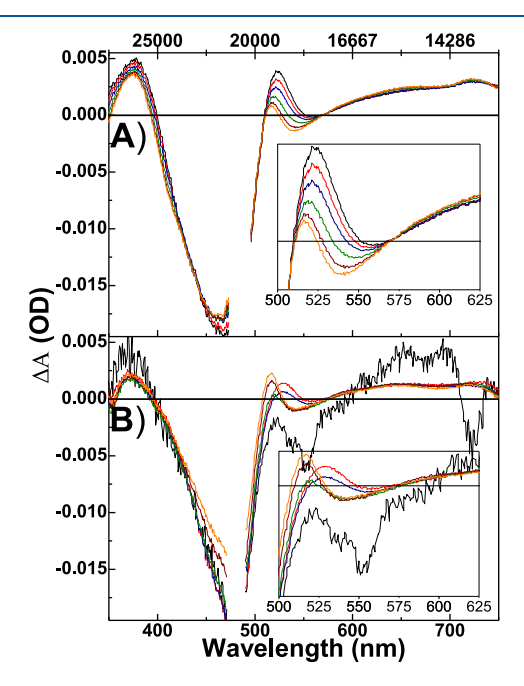


Figure 5. Ultrafast pump—probe transient absorption spectra for $[Cu(phen-4-1)_2]OTf$ (A) and $[Cu(phen-4-2)_2]OTf$ (B) collected in 1,2-dichloroethane. Insets: Enhanced 500 to 625 nm region for $[Cu(phen-4-1)_2]OTf$ and $[Cu(phen-4-2)_2]OTf$ to highlight spectral changes. The spectra are obtained at pump—probe delays of 0.3 ps (black), 0.75 ps (red), 2.5 ps (blue), 10 ps (green), 50 ps (brown), and 100 ps (orange).

respectively. The excited state features for $[Cu(phen-4-1)_2]^+$ and $[Cu(phen-4-2)_2]^+$ are similar to $[Cu(phen-2-1)_2]^+$ and $[Cu(phen-3-1)_2]^+$ for the most part consisting of two photoinduced ESA transitions from ~350 to 400 nm as well as from ~500 to 750 nm and a negative peak ranging from 400 to 500 nm. The assignment of the negative peak from 400 to 500 nm is to the GSB, the ESA from ~500 to 625 is the phen absorption, and 625 to 750 nm is the LMCT absorption. A notable difference is observed for the $[Cu(phen-4-1)_2]^+$ and $[Cu(phen-4-2)_2]^+$ compared with the $[Cu(phen-2-1)_2]^+$, and $[Cu(phen-3-1)_2]^+$ is a second negative absorption observed between 530 and 550 nm. Due to the low amplitude of this second negative absorption as well as the shaped phen ESA, we ascribe the second negative absorption to the tail of the

GSB overlapping with the reduced phen ESA. Time constants from the multiexponential fitting of the pump—probe transient absorption and nanosecond flash photolysis experiments are summarized in Table 1 with the data found in the Supporting Information (Figures S38 to S41).

In order to understand the results of the new complexes reported here, we found it necessary to collect spectroscopic data of the parent complex, $[Cu(dmp)_2](PF_6)$, for comparison. The electronic absorption spectrum of $[Cu(dmp)_2]^+$ features a broad transition with a maximum at 457 nm, a higher energy shoulder near 375 nm, and a tail from 500 to 600 nm. The emission spectrum displays a broad transition with a maximum near 750 nm. The excitation spectrum of $[Cu(dmp)_2]^+$ reveals a transition at 434 nm (blue-shifted relative to the absorption maxima) with a continuous intensity into the ultraviolet region. While many of the spectral features of the CF3-derivatized complexes are similar to that of the parent complex (see Figure 3), there is a noticeable difference in the intensity of the highest energy MLCT near 375 nm. Most notably, this transition has a much-reduced intensity in the CF₃ complexes. As we shall discuss later, the intensity of this peak is sensitive to the extent of excited-state distortion in the excited state. Pump-probe transient absorption spectra obtained at different time delays for [Cu(dmp)₂]⁺ (Figure 6B) also exhibit two ESA transitions from 350 to 400 nm and from 500 to 750 nm and a GSB ranging from 400 to 500 nm. The maxima of the two

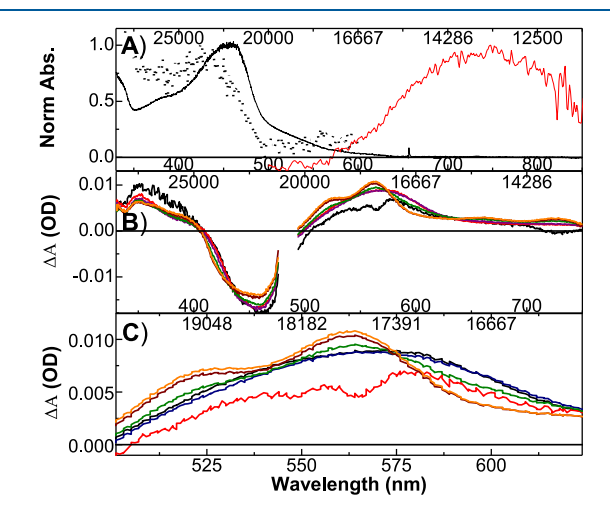


Figure 6. (A) Normalized electronic absorption (black solid line), emission (red solid line), and excitation (black scatter line) spectra for $[Cu(dmp)_2](PF_6)$ in 1,2-dichloroethane. (B) Ultrafast pump probe transient absorption spectra for $[Cu(dmp)_2]PF_6$ collected in 1,2-dichloroethane. (C) Enhanced 500 to 625 nm region for $[Cu(dmp)_2]PF_6$ collected in 1,2-dichloroethane. The selected spectra are taken at 0.3 ps (black), 0.75 ps (red), 2.5 ps (blue), 10 ps (green), 50 ps (brown), 100 ps (orange) time delays.

Table 2. Calculated Absorbance and the Dihedral Angle between Ligand Planes (Θ) for Select Ground and Excited States of $[Cu(NN)_2]^+$ Complexes

	$[Cu(dmp)_2]^+$	$[Cu(phen-2-1)_2]^+$	$[Cu(phen-3-1)_2]^+$	$[Cu(phen-4-1)_2]^+$	$[\operatorname{Cu}(\operatorname{phen-4-2})_2]^+$
calculated $\lambda_{max}(nm)$	461 nm	465 nm	467 nm	480 nm	482 nm
GS Θ	89.98°	90.00°	89.84°	89.98°	89.98°
N ^{th 1} MLCT	90.00°	90.00°	80.00°	89.97°	78.42°
¹ MLCT	63.92°	90.00°	78.29°	78.92°	80.27°
³ MLCT	62.93°	70.60°	74.92°	75.35°	74.38°

ESAs occur at 370 and 520 nm. The two ESA peaks from 500 to 625 nm are enhanced to highlight important spectral changes in the temporal response at these wavelengths (Figure 6C). Again, the lower energy ESA from \sim 625 to >750 nm is an LMCT absorption. The flash photolysis transient absorption spectra for [Cu(dmp)₂]⁺ also show the same features as the pump—probe spectra (Figure S30). Again, all time constants from the multiexponential fitting of the pump—probe transient absorption and nanosecond flash photolysis experiments are summarized in Table 1 with the data found in the Supporting Information (Figures S29 to S31). The steady-state absorption and emission, as well as time-resolved transient absorption experiments of [Cu(dmp)₂](PF₆), are consistent with previous reports.

DFT Calculations. Electronic-structure theory calculations have been performed on all five complexes listed in Scheme 1 using restricted and unrestricted density functional theory (DFT) in Gaussian 09 R.C.01.³⁴ All DFT methodology and benchmark discussion may be found in the Supporting Information. Unlike previous DFT calculations of Cu-(dmp)₂]⁺, which calculate the optimized structures as well as the potential energy surface as a function of θ , we have only performed structural optimizations of all five complexes for the ground state (S₀), ¹MLCT with the highest transition oscillator strength from the ground state (S_n), the lowest energy singlet excited state (S_1) , and the lowest energy triplet excited state (T_1) . Our intent is to correlate the θ at each stationary point to the observed transient absorption dynamics for a better insight on the effect CF₃ has on the excited state dynamics. The calculated absorption maxima and θ for each optimized structure are summarized in Table 2. We do recognize that previous calculations of $[Cu(dmp)_2]^+$ have predicted that θ for S_1 and T_1 is $\sim 70^\circ$, which is higher than our calculation of 62° , though all of our calculated trends agree with previous experiments.

DISCUSSION

Synthesis and Structural Characterization. Trifluoromethyl phenanthroline derivatives were synthesized via a hot radical method utilized by the authors.³⁵ This method is wellknown to produce a large number of compounds with a different number of substitutions and different substitution patterns, which in turn allows for the study of multiple compounds without the need to develop extensive multistep syntheses for each compound. We have previously shown that it is possible to trifluoromethylate another heteropolycyclic aromatic hydrocarbon, phenazine, with this method.³⁶ Phenanthroline derivatives with three and four trifluoromethyl substitutions were isolated from the reaction of CF₃I(g) and phenanthroline monohydrate in a sealed ampule. Isolation of the above compounds was achieved through multiple steps of HPLC. The isolation of derivatives with different numbers of substitutions, as well as derivatives with the same number of substitutions but different substitution patterns, allowed for a systematic study of the metal—ligand interaction.

To overcome the poor ligand strength of the tetra-substituted trifluoromethylated ligands, the copper(I) trifluoromethanesulfonate toluene complex was used as the copper(I) starting material. It was hypothesized that by using copper(I) trifluoromethanesulfonate toluene complex as the starting material, the combination of a weak anion and the very weakly coordinating toluene ligand would provide the right conditions for ligand exchange with the trifluoromethylated phenanthroline ligands. This reaction was performed with phen-4–1, phen-4–2, phen-3–1, and phen-2–1 to form the complexes [Cu(phen-4–1)₂]SO₃CF₃, [Cu(phen-4–2)₂]SO₃CF₃, [Cu(phen-3–1)₂]SO₃CF₃, and [Cu(phen-2–1)₂]SO₃CF₃, respectively.

The $[Cu(phen-4-1)_2]^+$ complex shown on the right in Figure 7 shows significantly more space being occupied by the

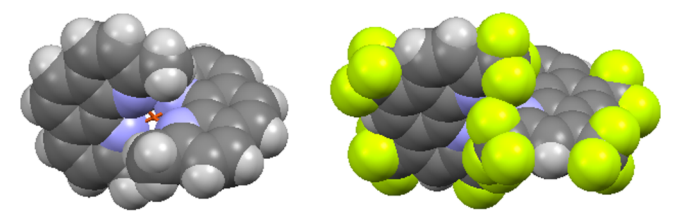


Figure 7. Space filling models of $[Cu(dmp)_2]^+$ (left)³⁷ and $[Cu(phen-4-1)_2]^+$ (right). Note the viewing angle has been moved to highlight the 2,9 substituents.

 ${\rm CF_3}$ groups in comparison to the ${\rm CH_3}$ groups in the ${\rm [Cu(dmp)_2]^+}$ complex. This likely has a significant impact on the pseudo-Jahn—Teller distortion that occurs in the excited state.

When comparing the Cu(I) complex single-crystal structures, the ligand dihedral angles decrease as more CF₃ groups are added. Kovalevsky et al. obtained crystal structures for [Cu(phen-2-1)₂]SO₃CF₃ in two different space groups.³⁰ The structure that has the space group $P2_1/c$ has a dihedral ligand angle of 89.5°, while the C2/c structure has a dihedral angle of 88.5°. The dihedral ligand angles for [Cu(phen-3-1)₂]SO₃CF₃ and [Cu(phen-4-1)₂]SO₃CF₃ decrease to 86.1° and 85.4°, respectively. It is likely that the 2,9-substituted CF₃ groups interact with CF₃ groups in the 4, 5, or 6 positions on the opposite ligand, causing the decrease in dihedral angle in the structure. While it is unlikely that this small change has such a dramatic effect, the decrease in dihedral ligand angle does correlate with the decreased excited-state lifetimes for the trifluoromethylated compounds as shown below.

Steady-State Absorption and Emission. The steady-state absorption and emission spectroscopy of $[Cu(NN)_2]^+$ are well documented to comprise multiple MLCT transitions ranging from 350 to 650 nm. The lowest energy MLCT transitions occur between 500 and 650 nm and are less intense

in comparison to the other CT transitions because they are formally forbidden in a pseudo T_d symmetry (where $\theta \approx 90^{\circ}$). These transitions are allowed in D_2 or lower symmetries (θ < 90°), with as little as 5° distortion from ideal T_d . The primary MLCT transitions are found from ~425 to 485 nm and are thought to be more intense due to the vibronic coupling of low energy Cu-N torsional modes to the electronic transition. The primary MLCT transitions are not symmetry forbidden as low energy transitions. Higher energy MLCT transitions are found from ~350 to ~425 nm and are symmetry forbidden similar to the low energy transitions in ideal T_d geometry. ^{6,15} The higher energy MLCT shoulder near 375 nm and low energy MLCT tail are highly sensitive to the degree of distortion in the Franck-Condon (FC) region, making them good spectral areas for comparison. In particular, the sharpness of the two primary MLCT transitions as seen in [Cu(phen-2-1)₂]+, $[Cu(phen-3-1)_2]^+$, and $[Cu(phen-4-1)_2]^+$ hint that minimal distortion occurs in the FC state as no higher energy shoulder is observed (Figure 3). This is unlike the [Cu(dmp),]+ and [Cu(phen-4-2)₂]⁺ complexes which feature a visibly broader and less resolved absorption spectrum. $[Cu(dmp)_2]^+$ has a well-documented subpicosecond time constant for excitedstate distortion.

As discussed in the Introduction, the emission maximum and QY are also important indicators of the excited-state distortion. The emission maximum and QY for the trifluoromethylated phen complexes for which emission could be collected as well as the dmp analogue exhibit a clear trend. Ordering the complexes starting with the highest energy emission and QY produces a sequence of [Cu(phen-2- $(1)_2$ ⁺, $[Cu(phen-3-1)_2]$ ⁺, and $[Cu(dmp)_2]$ ⁺. This emission trend is surprising as one may imagine from previous literature that the addition of a third CF₃ group ([Cu(phen-3-1)₂]+ complex) should exhibit a greater than or equal emission QY and Stokes shift relative to the $[Cu(phen-2-1)_2]^+$ complex (a ligand with two CF₃ groups).²⁹ Similarly, this same trend is also observed when comparing the excitation profiles to the absorption spectrum of [Cu(phen-2-1)₂]⁺, which overlap perfectly. However, the absorption spectra and excitation profile for $[Cu(dmp)_2]^+$ do not overlap, indicating a change in structure from the Franck-Condon state (initial structure open electronic absorption) and the emitting state. Thus, the absorption, excitation, and emission spectra of the CF₃ phenanthroline complexes indicate that these fluorinated ligands lead to a smaller pseudo-Jahn-Teller distortion relative to $[Cu(dmp)_2]^+$.

Numerous time-resolved experiments (absorption and emission), as well as DFT calculations, have been performed on [Cu(dmp)₂]⁺ and derivatives. The culmination of such experiments have made possible the assignments above in the Results section and outlined that the most prominent spectral and dynamic indicator for excited-state pseudo-Jahn-Teller distortion occurs in the GSB and phen regions. 14,16,17,25 Our discussion will focus heavily on the spectral shape and dynamics of these regions. Kinetic analysis of phen- ESA and GSB spectral regions reveals the presence of three time constants in [Cu(dmp)₂]⁺. A subpicosecond time constant, a tens of picoseconds time constant, and a long nanosecond time constant. The solvent dependence of the subpicosecond time constant as well as computational modeling has led to the assignment of an excited-state pseudo-Jahn-Teller distortion from $\sim T_d$ to D_2 (coincident with internal conversion).¹⁷ Coincident with the solvent dependence is an increase in the

intensity of the phen region in the first 1 ps following excitation, which further continues to blue shift, yielding a "double-peak" transition at 524 and 563 nm (Figure 6C). Likewise, the GSB dynamics depict an initial narrowing of the GSB from 460 to 500 nm in the first 2.5 ps followed by a subsequent blue shift. TDDFT calculations of singlet MLCT energy as a function of θ reveal that the energy of the third singlet state (S₃, state with the highest transition oscillator strength) increases as a function of θ . These calculations also indicate that the excited-state distortion occurs during internal conversion (IC) from the S₃ to S₁ (without a significant population of the S_2) with a time constant of ~ 300 fs. Similarly, the longer picosecond time constant is attributed to intersystem crossing (ISC) due to the lack of solvent dependence, TCSPC kinetics, and computational results, which reveal that the singlet-triplet energy gap increases as θ decreased from 90°. Moreover, other TDDFT ground-state projections of the singlet and triplet MLCT energy(s) demonstrate that as θ decreases from 90°, the ground state energy increases and the lowest triplet energy decreases, which together produces a large red shift in emission spectra. 15 All GSB and ESA features do eventually return to 0 with a time constant of 66.6 ± 2.1 ns, which is assigned as the electronhole recombination to regenerate the ground state complex (Figure S30).

On the basis of the steady-state absorption and emission comparison of [Cu(dmp)₂]⁺ with the CF₃ derivatives, we anticipated a number of differences in the shape of excited state spectra as well as dynamics. Indeed, a major difference is observed in the early spectra and kinetics of CF₃ complexes. The first resolved spectrum at 300 fs following excitation of [Cu(phen-2-1)₂]⁺ features a narrow single transition at 530 nm, while the [Cu(phen-3-1)₂]⁺ already shows a nicely resolved "double-peak." Both of these first spectra are unlike the broad ESA transition in $[Cu(dmp)_2]^+$ obtained at a similar pump-probe delay. Moreover, the transient spectra of $[Cu(phen-2-1)_2]^+$ and $[Cu(phen-3-1)_2]^+$ only show a modest increase in intensity with a smooth transition to the blue, producing multiple isosbestic points in the process (Figure 4A,B, inset). Further kinetic analysis of the [Cu(phen- $(2-1)_2^+$ and $[Cu(phen-3-1)_2^+]$ complexes do not reveal a subpicosecond kinetic phase in the phen ESA region (Table 1). The picosecond kinetics fit well to a single exponential process with time constants of 69 \pm 5 and 6.0 \pm 2.3 ps for $[Cu(phen-2-1)_2]^+$ and $[Cu(phen-3-1)_2]^+$, respectively. We suspect that the "double-peak" spectral signature of the phenis maintained at longer pump-probe delays but that the laser line obscures the higher energy peak. Likewise, the GSBs of $[Cu(phen-2-1)_2]^+$ and $[Cu(phen-3-1)_2]^+$ from 400 to 500 nm also show differences in comparison to $[\text{Cu}(\text{dmp})_2]^+.$ The GSBs of $[Cu(phen-2-1)_2]^+$ and $[Cu(phen-3-1)_2]^+$ do not exhibit narrowing or a shift in wavelength, whereas [Cu-(dmp)₂]⁺ shows both of these spectral changes. Furthermore, unlike the phen ESA where [Cu(phen-2-1)₂] and [Cu-(phen-3-1)₂]⁺ exhibit similar changes, the GSB of [Cu(phen-2-1)₂]⁺ and [Cu(phen-3-1)₂]⁺ displays large differences in the magnitude of the bleach recovery. The GSB of [Cu(phen- $(2-1)_2$ ⁺ is resolved by the first transient spectra at 300 fs and exhibits a 48% recovery (at 462 nm) with a time constant of 69 \pm 5 ps. The GSB of $[Cu(phen-3-1)_2]^+$ is also resolved by the first transient spectra at 300 fs though unlike [Cu(dmp)₂]⁺ and $[Cu(phen-2-1)_2]^+$, only a 5% recovery (462 nm) of the GSB is observed with a time constant of 6.0 \pm 2.3 ps. The single

wavelength kinetic time constants for the changes in the GSB as well as the phen⁻ ESA are displayed in Table 1. These differences in temporal and spectral response are undoubtedly due to differences in structural relaxation following MLCT excitation.

A more in-depth insight into these spectroscopic differences in the GSB kinetics may be explained by the DFT optimized structures. The excited state S_n and S₁ optimization of $[Cu(phen-2-1)_2]^+$ yields a θ of 90°, thus predicting that the distortion will occur during ISC (not during IC as seen in other Cu(I) complexes), which occurs between the S_1 (θ = 90°) and T_1 ($\theta = 70.6^\circ$). While higher lying triplet states are often involved during ISC, IC and vibrational redistribution in the triplet manifold are rapid, resulting in a thermalized T₁ excited state. In contrast, excited state optimization of [Cu(phen-3-1)₂]⁺ reveals that the distortion will begin from the initially prepared Franck-Condon ($\theta = 90^{\circ}$) states with most of this distortion occurring during adiabatic relaxation of S_n ($\theta = 80^\circ$) and then IC to S_1 ($\theta = 78.3^\circ$). A second smaller distortion occurs during ISC for T_1 ($\theta = 74.9^{\circ}$). On the basis of our earlier discussion of [Cu(dmp)₂]⁺ dynamics and DFT optimizations, we ascribe the single observed time constant in both $[Cu(phen-2-1)_2]^+$ and $[Cu(phen-3-1)_2]^+$ to ISC. As mentioned earlier, the pseudo-Jahn-Teller distortion in [Cu(phen-2-1)₂]⁺ is likely coincident with ISC as IC is predicted to be sub IRF, while in $[Cu(phen-3-1)_2]^+$ the distortion is coincident with IC, which occurs faster than our instrument response (earlier than 300 fs). The nanosecond flash photolysis of [Cu(phen-2-1)₂]⁺ and [Cu(phen-3-1)₂]⁺ exhibits the same unexpected trend as the emission results. Again, the $[Cu(phen-2-1)_2]^+$ has the longest observed lifetime followed by $[Cu(phen-3-1)_2]^+$ and $[Cu(dmp)_2]^+$ (Table 1). This trend is also contradictory to the calculated trend for θ where the T_1 of $[Cu(phen-3-1)_2]^+$ is less distorted than [Cu(phen-2-1)₂]⁺. The observed time-resolved dynamics and emission trend is that the addition of trifluoromethyl groups past two decreases the excited state lifetime. This suggests that previously observed trends of increased excited-state lifetime with increased steric bulk can be affected, and even reversed, when electron-withdrawing substituents are used.

Our observations of [Cu(phen-2-1)₂]⁺ and [Cu(phen-3- $[1]_2^+$ are consistent with earlier reports of $[Cu(phen-2-1)_2^+]_2^+$ where it was also noticed that the emission maxima and QY correlate with results for structurally inhibited complexes while the excited-state lifetime is much shorter.²⁴ For example, $[Cu(dsbp)_2]^+$ and $[Cu(dsbtmp)_2]^+$, where dsbp and dsbtmp are 2,9-di-sec-butyl-1,10-phenanthroline and 2,9-di-sec-butyl-2,3,7,8-tetramethyl-1,10-phenanthroline, reported by Castellano and co-workers, exhibit emission maxima of 690 and 631 nm, respectively, and QYs of 4.5×10^{-3} and 6.3×10^{-2} , respectively.³⁸ Transient absorption of these complexes yielded three kinetic time constants of 0.1–0.4 ps (τ_1) , 6–10 ps (τ_2) , and 380 ns (τ_3) for dsbp and 0.1–0.4 ps (τ_1) , 2–4 ps (τ_2) , and 2.8 μ s (τ_3) for dsbtmp complexes in dichloromethane. ^{25,38} They did not report θ for $[Cu(dsbp)_2]^+$. Surprisingly, while the emission maxima and quantum yield of [Cu(phen-2-1)₂]⁺ and [Cu(dsbp)₂]⁺ are nearly identical, the excited-state kinetics are substantially different. Recall that for $[Cu(phen-2-1)_2]^+$, τ_2 is 69 ps and $\tau_{\rm em}$ is 98 ns. Thus, while τ_2 is longer (representing ISC), the excited lifetime is not longer, suggesting that the potential energy surfaces for the CF₃ phen complexes are significantly different than the dialkylphenanthroline complexes.

Photodecomposition of the $[Cu(phen-4-1)_2]^+$ and [Cu- $(phen-4-2)_2$ complexes has excluded their inclusion in much of the discussion. We propose that the decomposition is caused primarily by the σ bond inductive withdrawing nature of CF3 groups on the coordinating phen nitrogen p orbitals making the phen-4-1 and phen-4-2 compounds worse coordinating ligands. This weak coordination is further evidenced by the longer Cu-N bond lengths of [Cu(phen- $(4-1)_2^+$ compared to $[Cu(phen-3-1)_2^+]$. Furthermore, a consequence of this weaker coordination is seen upon photoexcitation where any low energy Cu-N torsional or bond elongation is breaking the unreduced ligand bonds to copper, resulting in bond dissociation. This observation is consistent with trifluoromethylated bipyridine complexes of ruthenium(II) where tetra-trifluoromethylated bipyridine complexes could not be synthesized.³¹ Due to the decomposition of $[Cu(phen-4-1)_2]^+$ and $[Cu(phen-4-2)_2]^+$, the observed emission and excitation spectra of these complexes strongly resemble those of the free ligands (Figures S40, S42, and S44). The pump-probe transient absorption of both $[Cu(phen-4-1)_2]^+$ and $[Cu(phen-4-2)_2]^+$ complexes is reminiscent of [Cu(phen-2-1)₂]⁺. We note clean isosbestic points at 507 and 573 nm for [Cu(phen-4-1)₂]⁺ (Figure 5A, inset), while the [Cu(phen-4-2)₂]⁺ complex (Figure 5B, inset) does not have any isosbestic points in the phen region. As mentioned in the Results section, the strong ground-state overlap with the ESA distorts the phen double peak. The formation of the bleach at ~540 nm occurs concomitantly with the blue shift in $[Cu(phen-4-1)_2]^+$ and $[Cu(phen-4-2)_2]^+$ ESA. Surprisingly, the GSB region of $[Cu(phen-4-1)_2]^+$ and $[Cu(phen-4-2)_2]^+$ does not exhibit any major spectral changes on the picosecond time scale, hinting that all the spectral differences originate from the ESA. The kinetic analysis of the single time constant for $[Cu(phen-4-1)_2]^+$ is consistent with $[Cu(phen-3-1)_2]^+$ and is assigned to ISC. Unlike all other CF₃ complexes, the $[Cu(phen-4-2)_2]^+$ features important differences. As mentioned in the steady-state results section, the electronic absorption of $[Cu(phen-4-2)_2]^+$ shares more similarities with [Cu(dmp)₂]⁺ than trifluoromethyl complexes. The pump-probe transient absorption kinetics also have observable differences. The single wavelength as well as global fitting kinetic of $[Cu(phen-2-1)_2]^+$, $[Cu(phen-3-1)_2]^+$, and [Cu(phen-4-1)₂]⁺ all exhibit one time constant on the ultrafast time scale, yet a second short time constant is only observed in single wavelength fitting of [Cu(phen-4-2)₂] (Table 1). The \sim 4 ps time constant is observed in the excitedstate regions when fitting in single wavelengths, however, is not necessary to acquire good early time agreement in the global fitting analysis (Figure S41). The assignment of the ~4 ps time constant is ISC with the 160 ps assigned as a bifurcation leading to decomposition. Again, only a single nanosecond flash photolysis and time correlated single wavelength kinetics could be obtained for the $[Cu(phen-4-1)_2]^+$ (Figure S39) and no flash photolysis data for $[Cu(phen-4-2)_2]^+$. The observed lifetime for $[Cu(phen-4-1)_2]^+$ is 17 ns, which is shorter than the excited state lifetime of the other copper complexes (>66 ns; Table 1). This result is unexpected as the decreased excited-state distortion observed in the ground state absorption and DFT excited state optimized structures would suggest a long-lived excited-state lifetime of the copper complex. The observation of the shorter lifetime is attributed to an observed rate of the photodecomposition reaction in the [Cu(phen-4-

 $(1)_2$ to the ground state.

CONCLUSION

We have reported the synthesis and characterization of trifluoromethyl copper(I) phenanthroline complexes. In aggregate, the sum total of the steady state spectra, timeresolved experimentation, and DFT calculations all point to inhibition of excited state pseudo-Jahn-Teller distortion from the substitution of the 2,9 methyl groups for the trifluoromethyl groups. Our finding resembles previous observations of copper(I) complexes with enhanced bulk in the 2,9 phen positions with the caveat that the trifluoromethylation changes the potential energy surface to favor $\theta \sim 90^{\circ}$. If trifluoromethylation simply enhanced the steric bulk restricting pseudo-Jahn-Teller distortion, then we would expect similar emission maxima, emission QY, and ns flash photolysis lifetimes for all complexes which are not experimentally observed. The observed time-resolved dynamics and emission trend that the addition of trifluoromethyl groups past two decreases the excited-state lifetime is contrary to the traditional understanding of [Cu(NN)₂]⁺ complexes. Static single reference optimizations of select excited state structures further corroborate these observations. In aggregate, these results outline the need for further high level dynamic theory computations and experimental vibrational investigation into copper(I) complexes where the 2,9 phen position constituents alter both the sterics and electronics of the excited state.

ASSOCIATED CONTENT

Supporting Information

The Supporting Information is available free of charge at https://pubs.acs.org/doi/10.1021/acs.inorgchem.9b03146.

 1 H and 19 F NMR spectra of trifluoromethyl $[Cu(NN)_{2}]^{+}$ complexes, full description of instrumentation, DFT methodology and benchmarking, representative single wavelength kinetic and global kinetic fitting for ultrafast pump—probe experiments for all complexes, representative single wavelength kinetic and global kinetic fitting for ns flash photolysis experiments for all complexes, excitation, and emission of $[Cu(phen-4-1)_{2}]^{+}$, $[Cu-(phen-4-2)_{2}]^{+}$, and dmp ligand (PDF)

Accession Codes

CCDC 1964414–1964415 contain the supplementary crystallographic data for this paper. These data can be obtained free of charge via www.ccdc.cam.ac.uk/data_request/cif, or by emailing data_request@ccdc.cam.ac.uk, or by contacting The Cambridge Crystallographic Data Centre, 12 Union Road, Cambridge CB2 1EZ, UK; fax: +44 1223 336033.

AUTHOR INFORMATION

Corresponding Authors

Olga V. Boltalina — Department of Chemistry, Colorado State University, Fort Collins, Colorado 80523, United States; Email: olga.boltalina@colostate.edu

Jeffrey J. Rack — Department of Chemistry and Chemical Biology, The University of New Mexico, Albuquerque, New Mexico 87131, United States; ⊚ orcid.org/0000-0001-6121-879X; Email: jrack@unm.edu

Authors

Maksim Y. Livshits — Department of Chemistry and Chemical Biology, The University of New Mexico, Albuquerque, New Mexico 87131, United States; ⊙ orcid.org/0000-0003-3601-1230

Brian J. Reeves — Department of Chemistry, Colorado State University, Fort Collins, Colorado 80523, United States

Nicholas J. DeWeerd — Department of Chemistry, Colorado State University, Fort Collins, Colorado 80523, United States

Steven H. Strauss — Department of Chemistry, Colorado State University, Fort Collins, Colorado 80523, United States;

orcid.org/0000-0001-7636-2671

Complete contact information is available at: https://pubs.acs.org/10.1021/acs.inorgchem.9b03146

Notes

The authors declare no competing financial interest.

ACKNOWLEDGMENTS

J.J.R. acknowledges NSF (Grant CHE 1602240) and UNM startup for financial support. S.H.S. and O.V.B. acknowledge NSF (grant CHE 1362302) for partial financial support. UNM Center for Advanced Research Computing (CARC) for access to Gaussian 09 R.C.01 and Gausview 5.0.1. Invaluable assistance by Dr. Yu Sheng Chen of Argonne National Laboratory, USA in the X-ray crystallography experiments is appreciated.

REFERENCES

- (1) Bessho, T.; Constable, E. C.; Graetzel, M.; Hernandez Redondo, A.; Housecroft, C. E.; Kylberg, W.; Nazeeruddin, M. K.; Neuburger, M.; Schaffner, S. An element of surprise—efficient copper-functionalized dye-sensitized solar cells. *Chem. Commun.* **2008**, No. 32, 3717—3710
- (2) Lv, L.; Liu, K.; Yuan, K.; Zhu, Y.; Wang, Y. Thermally activated delayed fluorescence processes for Cu(i) complexes in solid-state: a computational study using quantitative prediction. *RSC Adv.* **2018**, 8 (50), 28421–28432.
- (3) Sandroni, M.; Kayanuma, M.; Planchat, A.; Szuwarski, N.; Blart, E.; Pellegrin, Y.; Daniel, C.; Boujtita, M.; Odobel, F. First Application of the HETPHEN Concept to New Heteroleptic Bis(diimine) Copper(I) Complexes as Sensitizers in Dye Sensitized Solar Cells. *Dalton Trans.* **2013**, 42 (30), 10818–10827.
- (4) Ahn, B.-T.; McMillin, D. R. Studies of Photoinduced Electron transfer from Bis(2,9-dimethyl-1,10-Phenanthroline)Copper(I). *Inorg. Chem.* 1978, 17 (8), 2253–2258.
- (5) McMillin, D. R.; Buckner, M. T.; Ahn, B. T. A Light-Induced Redox Reaction of Bis(2,9-dimethyl-1,10-phenanthroline)Copper(I). *Inorg. Chem.* 1977, 16 (4), 943–945.
- (6) Blaskie, M. W.; McMillin, D. R. Photostudies of Copper(I) Systems. 6. Room-Temperature Emission and Quenching Studies of Bis(2,9-dimethyl-1,10-Phenanthroline)Copper(I). *Inorg. Chem.* **1980**, 19 (11), 3519–3522.
- (7) Mara, M. W.; Fransted, K. A.; Chen, L. X. Interplays of Excited State Structures and Dynamics in Copper(I) Diimine Complexes: Implications and Perspectives. *Coord. Chem. Rev.* **2015**, 282–283, 2–18.
- (8) Prier, C. K.; Rankic, D. A.; MacMillan, D. W. C. Visible Light Photoredox Catalysis with Transition Metal Complexes: Applications in Organic Synthesis. *Chem. Rev.* **2013**, *113* (7), 5322–5363.
- (9) Wagenknecht, P. S.; Ford, P. C. Metal Centered Ligand Field Excited States: Their Roles in the Design and Performance of Transition Metal Based Photochemical Molecular Devices. *Coord. Chem. Rev.* **2011**, 255 (5), 591–616.
- (10) Auböck, G.; Chergui, M. Sub-50-fs Photoinduced Spin Crossover in [Fe(bpy)3]2+. *Nat. Chem.* **2015**, 7 (8), 629–633.

- (11) Kober, E. M.; Meyer, T. J. An Electronic Structural Model for the Emitting MLCT Excited States of Ru(bpy)₃²⁺ and Os(bpy)₃²⁺. *Inorg. Chem.* **1984**, 23, 3877–3886.
- (12) Yaghoobi Nia, N.; Farahani, P.; Sabzyan, H.; Zendehdel, M.; Oftadeh, M. A Combined Computational and Experimental Study of the [Co(bpy)3]2+/3+ Complexes as One-Electron Outer-Sphere Redox Couples in Dye-Sensitized Solar Cell Electrolyte Media. *Phys. Chem. Chem. Phys.* **2014**, *16* (23), 11481–11491.
- (13) Buckner, M. T.; McMillin, D. R. Photoluminescence from Copper(I) Complexes with Low-Lying Metal-to-Ligand Charge Transfer Excited States. *J. Chem. Soc., Chem. Commun.* 1978, No. 17, 759–761.
- (14) Palmer, C. E. A.; McMillin, D. R.; Kirmaier, C.; Holten, D. Flash Photolysis and Quenching Studies of Copper(I) Systems in the Presence of Lewis Bases: Inorganic exciplexes? *Inorg. Chem.* **1987**, 26 (19), 3167–3170.
- (15) Siddique, Z. A.; Yamamoto, Y.; Ohno, T.; Nozaki, K. Structure-Dependent Photophysical Properties of Singlet and Triplet Metal-to-Ligand Charge Transfer States in Copper(I) Bis(diimine) Compounds. *Inorg. Chem.* **2003**, *42* (20), *6366–6378*.
- (16) Chen, L. X.; Shaw, G. B.; Novozhilova, I.; Liu, T.; Jennings, G.; Attenkofer, K.; Meyer, G. J.; Coppens, P. MLCT State Structure and Dynamics of a Copper(I) Diimine Complex Characterized by Pump-Probe X-ray and Laser Spectroscopies and DFT Calculations. *J. Am. Chem. Soc.* 2003, 125 (23), 7022–7034.
- (17) Shaw, G. B.; Grant, C. D.; Shirota, H.; Castner, E. W.; Meyer, G. J.; Chen, L. X. Ultrafast Structural Rearrangements in the MLCT Excited State for Copper(I) bis-Phenanthrolines in Solution. *J. Am. Chem. Soc.* **2007**, 129 (7), 2147–2160.
- (18) Du, L.; Lan, Z. Ultrafast Structural Flattening Motion in Photoinduced Excited State Dynamics of a Bis(diimine) Copper(I) Complex. Phys. Chem. Chem. Phys. 2016, 18 (11), 7641–7650.
- (19) Iwamura, M.; Takeuchi, S.; Tahara, T. Ultrafast Excited-State Dynamics of Copper(I) Complexes. *Acc. Chem. Res.* **2015**, 48 (3), 782–791.
- (20) Brown-Xu, S.; Fumanal, M.; Gourlaouen, C.; Gimeno, L.; Quatela, A.; Thobie-Gautier, C.; Blart, E.; Planchat, A.; Riobé, F.; Monnereau, C.; Chen, L. X.; Daniel, C.; Pellegrin, Y. Intriguing Effects of Halogen Substitution on the Photophysical Properties of 2,9-(Bis)halo-Substituted Phenanthrolinecopper(I) Complexes. *Inorg. Chem.* **2019**, 58 (12), 7730–7745.
- (21) Soulis, K.; Gourlaouen, C.; Daniel, C.; Quatela, A.; Odobel, F.; Blart, E.; Pellegrin, Y. New luminescent copper(I) complexes with extended π -conjugation. *Polyhedron* **2018**, *140*, 42–50.
- (22) Everly, R. M.; Ziessel, R.; Suffert, J.; McMillin, D. R. Steric Influences on the Photoluminescence from Copper(I) Phenanthrolines in Rigid Media. *Inorg. Chem.* **1991**, *30* (3), 559–561.
- (23) Ichinaga, A. K.; Kirchhoff, J. R.; McMillin, D. R.; Dietrich-Buchecker, C. O.; Marnot, P. A.; Sauvage, J. P. Charge-Transfer Absorption and Emission of Cu(NN)2+ Systems. *Inorg. Chem.* **1987**, 26 (25), 4290–4292.
- (24) Cunningham, C. T.; Cunningham, K. L. H.; Michalec, J. F.; McMillin, D. R. Cooperative Substituent Effects on the Excited States of Copper Phenanthrolines. *Inorg. Chem.* 1999, 38 (20), 4388–4392.
- (25) McCusker, C. E.; Castellano, F. N. Design of a Long-Lifetime, Earth-Abundant, Aqueous Compatible Cu(I) Photosensitizer Using Cooperative Steric Effects. *Inorg. Chem.* **2013**, 52 (14), 8114–8120.
- (26) Lockard, J. V.; Kabehie, S.; Zink, J. I.; Smolentsev, G.; Soldatov, A.; Chen, L. X. Influence of Ligand Substitution on Excited State Structural Dynamics in Cu(I) Bisphenanthroline Complexes. *J. Phys. Chem. B* **2010**, *114* (45), 14521–14527.
- (27) Brunner, F.; Klein, Y. M.; Keller, S.; Morris, C. D.; Prescimone, A.; Constable, E. C.; Housecroft, C. E. The beneficial effects of trifluoromethyl-substituents on the photoconversion efficiency of copper(i) dyes in dye-sensitized solar cells. *RSC Adv.* **2015**, *5* (72), 58694–58703.
- (28) Benari, M. D.; Hefter, G. T. Electrochemical Characteristics of the Copper(II)-Copper(I) Redox Couple in Dimethyl Sulfoxide Solutions. *Aust. J. Chem.* **1990**, *43* (11), 1791–1801.

- (29) Miller, M. T.; Gantzel, P. K.; Karpishin, T. B. A Photoluminescent Copper(I) Complex with an Exceptionally High CuII/CuI Redox Potential: [Cu(bfp)2]+ (bfp = 2,9-bis(trifluoromethyl)-1,10-phenanthroline). *Angew. Chem., Int. Ed.* **1998**, 37 (11), 1556–1558
- (30) Kovalevsky, A. Y.; Gembicky, M.; Coppens, P. Cu(I)(2,9-Bis(trifluoromethyl)-1,10-phenanthroline)2+ Complexes: Correlation between Solid-State Structure and Photoluminescent Properties. *Inorg. Chem.* **2004**, *43* (26), 8282–8289.
- (31) Furue, M.; Maruyama, K.; Oguni, T.; Naiki, M.; Kamachi, M. Trifluoromethyl-Substituted 2,2'-Bipyridine Ligands. Synthetic Control of Excited-State Properties of Ruthenium(II) Tris-Chelate Complexes. *Inorg. Chem.* **1992**, 31 (18), 3792–3795.
- (32) Beer, R. H.; Jimenez, J.; Drago, R. S. Syntheses of 2,9-bis(halomethyl-1,10-phenanthrolines: potential robust ligands for metal oxidation catalysts. *J. Org. Chem.* **1993**, 58 (7), 1746–1747.
- (33) Gordon, K. C.; McGarvey, J. J. Time-Resolved Resonance Raman Spectroscopy of Bis(2,9-dimethyl-1,10-phenanthroline)-Copper(1+) in Solution. *Inorg. Chem.* **1991**, 30 (15), 2986–2989.
- (34) Frisch, M. J.; Trucks, G. W.; Schlegel, H. B.; Scuseria, G. E.; Robb, M. A.; Cheeseman, J. R.; Scalmani, G.; Barone, V.; Mennucci, B.; Petersson, G. A.; Nakatsuji, H.; Caricato, M.; Li, X.; Hratchian, H. P.; Izmaylov, A. F.; Bloino, J.; Zheng, G.; Sonnenberg, J. L.; Hada, M.; Ehara, M.; Toyota, K.; Fukuda, R.; Hasegawa, M. I.; Nakajima, T.; Honda, Y.; Kitao, O.; Nakai, H.; Vreven, T.; Montgomery, J. A.; Peralta, J. J. E.; Ogliaro, F.; Bearpark, M.; Heyd, J. J.; Brothers, E.; Kudin, K. N.; Staroverov, V. N.; Keith, T.; Kobayashi, R.; Normand, J.; Raghavachari, K.; Rendell, A.; Burant, J. C.; Iyengar, S. S.; Tomasi, J.; Cossi, M.; Rega, N.; Millam, J. M.; Klene, M.; Knox, J. E.; Cross, J. B.; Bakken, V.; Adamo, C.; Jaramillo, J.; Gomperts, R.; Stratmann, R. E.; Yazyev, O.; Austin, A. J.; Cammi, R.; Pomelli, C.; Ochterski, J. W.; Martin, R. L.; Morokuma, K.; Zakrzewski, V. G.; Voth, G. A.; Salvador, P.; Dannenberg, J. J.; Dapprich, S.; Daniels, A. D.; Farkas, O.; Foresman, J. B.; Ortiz, J. V.; Cioslowski, J.; Fox, D. J. Gaussian 09, Rev. C01; Gaussian Inc.: Wallingford, CT, 2010.
- (35) Kuvychko, I. V.; Castro, K. P.; Deng, S. H. M.; Wang, X.-B.; Strauss, S. H.; Boltalina, O. V. Taming Hot CF3 Radicals: Incrementally Tuned Families of Polyarene Electron Acceptors for Air-Stable Molecular Optoelectronics. *Angew. Chem., Int. Ed.* **2013**, *52* (18), 4871–4874.
- (36) Castro, K. P.; Clikeman, T. T.; DeWeerd, N. J.; Bukovsky, E. V.; Rippy, K. C.; Kuvychko, I. V.; Hou, G.-L.; Chen, Y.-S.; Wang, X.-B.; Strauss, S. H.; Boltalina, O. V. Incremental Tuning Up of Fluorous Phenazine Acceptors. *Chem. Eur. J.* **2016**, 22 (12), 3930–3936.
- (37) Kovalevsky, A. Y.; Gembicky, M.; Novozhilova, I. V.; Coppens, P. Solid-State Structure Dependence of the Molecular Distortion and Spectroscopic Properties of the Cu(I) Bis(2,9-dimethyl-1,10-phenanthroline) Ion. *Inorg. Chem.* **2003**, 42 (26), 8794–8802.
- (38) Garakyaraghi, S.; Danilov, E. O.; McCusker, C. E.; Castellano, F. N. Transient Absorption Dynamics of Sterically Congested Cu(I) MLCT Excited States. *J. Phys. Chem. A* **2015**, *119* (13), 3181–3193.